Nanoparticulate ceria–zirconia anode materials for intermediate temperature solid oxide fuel cells using hydrocarbon fuels

Shidong Song,† Rodolfo O. Fuentes‡ and Richard T. Baker*

Received 3rd June 2010, Accepted 17th August 2010
DOI: 10.1039/c0jm01741h

Solid Oxide Fuel Cells (SOFCs) represent an attractive technology for the conversion of chemical to electrical energy because of their high efficiencies and low environmental impact, and because of the useful, high grade heat also generated. Direct utilisation of hydrocarbons in SOFCs would contribute to the more sparing utilisation of remaining fossil fuel reserves. In the longer term, this technology could be extended to work with more sustainable biofuel and waste-derived feedstocks. In this work, nanoparticulate Ceria–Zirconia mixed oxides, $Ce_{1-x}Zr_xO_2$ ($x = 0.1$, 0.25, 0.5, 0.75 and 0.9), were studied with a view to their application as anode materials in intermediate temperature (IT) SOFCs using hydrocarbon fuels. Impedance spectra were recorded in symmetrical cells under reducing conditions using gadolinium-doped ceria (GDC) as the electrolyte material. The spectra were analysed in terms of a double fractal finite length Gerischer impedance model. The model parameters were found to have monotonic dependences on temperature and more complex relationships with respect to Zr content. Diffusion-related processes and the electrochemical reaction were fastest for intermediate Zr contents while the chemical exchange reaction rate increased with decreasing Zr content. As a result, anode catalysts with 10 and 25 mol% Zr showed the lowest polarisation resistances of only 0.17 and 4.52 Ω cm^2 at 700 °C in humidified 5% H_2 and humidified 5% CH_4, respectively. These values represented an approximately two-fold improvement on the pure ceria electrode. This performance compares very favourably with the currently most promising candidate anode materials applied in SOFCs for use with hydrocarbon fuels.

1. Introduction

Solid Oxide Fuel Cells (SOFCs) are of great interest as electrical power generation systems since they allow chemical potential energy to be converted directly into electrical energy with high efficiency and low emission of pollutants. Most SOFCs are based on ceramic oxygen ion conducting electrolytes and one of their most promising characteristics, in contrast to some other types of fuel cell, is the possibility of performing direct electrochemical oxidation of hydrocarbons. However, the conventional fuel electrode (anode) materials—composites, or cermets, of Ni–YSZ—cannot satisfy this application because of the activity of Ni for hydrocarbon cracking, which results in the formation of carbonaceous deposits, and because of the oxidation of Ni to NiO by steam and CO_2, both processes which cause a performance degradation of the anode.[1] Therefore, anode materials which can withstand the high temperatures and redox cycling of SOFC operation whilst also catalysing electrochemical oxidation of hydrocarbon fuels are in demand.

Ceria-based materials have been developed as very promising alternatives for avoiding carbon deposition and have been demonstrated to work successfully on methane and some other gaseous and liquid hydrocarbons.[2,3] Gorte and co-workers have published a series of papers on the use of Cu–ceria cermet for the direct utilization of a wide range of hydrocarbon fuels in SOFCs at operating temperatures below 800 °C.[4–7] In these anodes, Cu was chosen as the electronic conductor due to its catalytic inertness for C–C bond breaking and coke formation. The ceria component acted as an oxidation catalyst and a mixed ionic–electronic conductor (MIEC) under reducing conditions. However, the main weakness of ceria is its low thermal stability under SOFC preparation and operating conditions. He *et al.*[8] found ceria to be strongly affected by calcination temperature. The Area-Specific Resistance (ASR) of a ceria-based SOFC using H_2 at 973 K was about 3 times higher when the ceria had been calcined at 1523 K rather than at 723 K. This was attributed to loss of ceria surface area resulting from particle sintering.

Ceria has been widely applied as a redox or oxygen storage promoter in automotive three-way catalysts (TWCs). In TWCs, the thermal stability of ceria is improved by doping with zirconia.[9] In addition, the dissolution of ZrO_2 into the cubic fluorite lattice of CeO_2 strongly affects its catalytic behaviour by lowering the activation energy for mobility of oxygen ions within the lattice. This results in an increase in the bulk oxygen mobility and the oxygen storage capacity (OSC) and leads to an improvement in the redox properties of the material.[9,10] Larrondo *et al.*[11] studied the catalytic activity of Ce/Zr mixed oxides for direct oxidation of methane using the Temperature Programmed Reduction (TPR) technique with a view to their potential application as anode materials in SOFCs. They reported that Zr can improve the reducibility of both surface and

EaStChem, School of Chemistry, University of St Andrews, North Haugh, St Andrews, Fife, KY16 9ST, UK. E-mail: rtb5@st-andrews.ac.uk
† Present address: School of Chemical and Environmental Engineering, China University of Mining and Technology, Beijing 100083, P.R. China.
‡ Present address: CINSO (Solid State Research Centre), CONICET-CITEFA, J.B. de La Salle 4397, Villa Martelli, B1603ALO, Buenos Aires, Argentina.

bulk ceria sites. In the Ce/Zr oxides they studied, the catalyst with 10 mol% Zr showed higher methane conversion than the other compositions over the whole temperature range used. Ahn *et al.*[12] compared the performance of Cu–$Ce_{0.6}Zr_{0.4}O_2$–YSZ and Cu–CeO_2–YSZ as the anode material in an SOFC. The latter showed the better performance when both anode materials were calcined at the low temperature of 723 K. However, the situation was reversed after calcination at 1273 K, showing that doping with Zr can improve the thermal stability of the anode. This is an important factor since repeated thermal cycling is likely in many practical SOFC applications.

In addition to the potential for loss of CeO_2 surface area through sintering, another limitation of Cu–CeO_2-based anodes is the relatively low melting temperature of Cu. This can make the fabrication of Cu cermets difficult and also limits the SOFC operation temperature to below 800 °C in order to avoid the agglomeration of Cu particles. To reduce SOFC operating temperatures significantly below typical values of ~900 °C, the resistance of the electrolyte to the flow of oxygen ions must be decreased. This can be done both by reducing the thickness of the electrolyte layer (to ~10 μm) and by using materials with very high oxygen ion conductivities. In this way, cells working at intermediate temperature—IT-SOFCs—can be developed. The development of IT-SOFCs capable of utilizing hydrocarbon fuels directly would have many advantages, including allowing their housings to be made from conventional construction materials rather than high cost ceramics. Furthermore, highly oxygen ion conducting electrolytes may also benefit the catalytic activity of the anode. Lu *et al.*[13] studied SOFCs using several IT electrolytes of current interest, including samaria-doped ceria (SDC), Sr and Mg-doped lanthanum gallate (LSGM) and scandia-stabilized zirconia (ScSZ), all with the same composite Cu–ceria anodes. The results showed that the use of such IT electrolytes with high ionic conductivity can improve the anode performance. The authors attributed this benefit to improved ionic transport in the anode. The best results at 700 °C were for the cell using an SDC electrolyte.

Though important studies on the ceria-based anodes have been reported, the systematic study of Ce/Zr mixed oxides as anode materials, especially the application of such materials in SOFCs with IT-electrolytes, is an area that should be further addressed. In the present work, we investigated the performance of $Ce_{1-x}Zr_xO_2$ ($x = 0.1$, 0.25, 0.5, 0.75 and 0.9) as anode materials in symmetrical cells with gadolinium doped ceria (GDC) electrolytes at intermediate temperatures under humidified H_2 and humidified CH_4 by impedance spectroscopy (IS). Using GDC instead of YSZ as the electrolyte gave the advantages of higher electrolyte conductivity and better adhesion and thermal and chemical matching to the $Ce_{1-x}Zr_xO_2$ materials, at least at the higher Ce contents. In order to allow relatively simple interpretation of IS spectra, and to avoid potential errors caused by the location of a reference electrode, the IS experiments were carried out in a symmetrical cell—that is with the anode material and fuel gas at both electrodes—and in a two electrode configuration. It was found that the IS spectra fitted very well to an equivalent circuit model which included a double-fractal finite length Gerischer impedance. The fitting parameters are related to the physical properties of the cell components. Plotting the variation of these parameters with temperature and with anode composition (x) provided further insight into the performance of these materials as SOFC anodes.

Several researchers have observed a Gerischer response in the IS spectra of symmetrical electrochemical cells. Boukamp *et al.*[14,15] examined the impedances of symmetrical cells with Ni/Ti- and Tb-doped YSZ cermet anodes and found the impedance spectrum consisted of a small feature corresponding to the electrochemical reaction in the high frequency region and a dominant finite length Gerischer response in the low frequency region. The Gerischer impedance was thought to be related to surface or bulk diffusion of oxygen species in competition with oxygen uptake/release through a (non-electro)chemical surface exchange reaction at the anode surface. An expression for the double-fractal finite length Gerischer (FFL-G) impedance was provided by these authors[15,16] and is given in eqn (1).

$$Z_{\text{FFL-G}}(\omega) = \frac{Z_O \tan h\left(L[k + (j\omega)^n]^\alpha \Big/ \sqrt{\tilde{D}_O}\right)}{\sqrt{\tilde{D}_O}[k + (j\omega)^n]^\alpha} \quad (1)$$

L is the diffusion length (cm), $\tilde{D}_O$ is the chemical diffusion coefficient of oxygen ions ($cm^2\ s^{-1}$), k is the rate constant of the oxygen uptake/release reaction ($s^{-1}\ cm^{-2}$), ω is angular frequency, n and α are fractal factors and Z_O is the characteristic resistance (ohm) defined by these authors as

$$Z_O = \frac{RTW}{4F^2 c_O} \quad (2)$$

where R, T and F have their usual meanings, c_O is the oxygen ion concentration in the mixed conducting electrode material and W is the thermodynamic enhancement factor (no units). W is a measure of the degree of departure of a system from the ideal statistics of a dilute solution of the diffusing species, for which $W = 1$. Generally expressed, the chemical diffusion coefficient, $\tilde{D}$, relates the flux of a diffusing species, J, to the gradient in its concentration, n, over distance, x, in Fick's law,

$$J = -\tilde{D}\frac{dn}{dx} \quad (3)$$

The thermodynamic enhancement factor, W, relates the chemical diffusion coefficient, $\tilde{D}$, to the 'jump' (or self-) diffusion coefficient, D_J, through

$$\tilde{D} = WD_J \quad (4)$$

and can be further related to the tracer diffusion coefficient, D^*, which applies in isotope studies, using the expression

$$\tilde{D} = W\frac{D^*}{H} \quad (5)$$

where H is the Haven ratio and has a value less than 2 for stable solid solutions.[17]

The Gerischer, or chemical, impedance is extensively treated by Adler[18] and a useful discussion of diffusion is provided by Bisquert.[17]

By using a FFL-G impedance model Boukamp and Bouwmeester[15,16] achieved a significantly better match between model and experimental data than by using other impedance elements.

2. Experimental

Preparation of GDC and $Ce_{1-x}Zr_xO_2$ oxides

All reagents used in this work were obtained from Alfa Aesar. GDC of composition $Ce_{0.9}Gd_{0.1}O_{1.95}$ was prepared following a low temperature chemical method established in the group.[19] $Ce(NO_3)_3 \cdot 6H_2O$ and $Gd(NO_3)_3 \cdot mH_2O$ were dissolved in deionised water individually and then mixed and stirred thoroughly. Citric acid was dissolved in deionised water and added to the nitrate solution. The molar ratio of total metal ions to citric acid was 1 : 2. After drying on a hotplate at 80 °C, a viscous gel was obtained. This was heated in air in a muffle furnace at 250 °C for 1 h. The resulting ash-like product was further calcined in air at 500 °C for 1 h in order to eliminate carbonaceous residues. Finally, the as-prepared GDC powder was dry-ground in nylon containers using a planetary ball mill operating at 400 rpm for 1 h. A similar procedure was used in the preparation of the $Ce_{1-x}Zr_xO_2$ powders. $Ce(NO_3)_3 \cdot 6H_2O$ and $ZrO(NO_3)_2 \cdot nH_2O$ were used as the starting reagents. Electron microscope images of typical $Ce_{1-x}Zr_xO_2$ starting powders are given in Fig. 1. The preparation method was chosen because gas bubbles are generated during the crystallisation step, giving rise to unusual paper-like sheets which, importantly, consisted of nanoparticles, as seen in Fig. 1a–c. Fig. 1c and d show that these nanoparticles were about 5 nm in diameter and were highly crystalline. The powders were ground before use to break up the layer structures and release the nanocrystals. The preparation of these powders is described in detail elsewhere.[20] The final oxides were named according to their equivalent Zirconia content in mol%. Thus Z10DC represented a sample with 10 mol% of ZrO_2 in ceria, *i.e.* $Ce_{0.9}Zr_{0.1}O_2$. Samples with 0, 10, 25, 50, 75 and 90 mol% ZrO_2 were prepared.

Preparation of symmetrical cells

The GDC powders were uniaxially pressed into cylindrical pellets at a pressure of 200 MPa and sintered in air at 1450 °C for 8 h. The final dimensions of these GDC electrolyte pellets were 0.9 mm in thickness and 19 mm in diameter. Each ZDC oxide was mixed with a homemade organic vehicle and carbon-based pore former using a ball mill for 20 h to form a uniform slurry. This was deposited onto each side of the GDC pellet by screen printing to form two identical electrode layers. The geometrical area of each electrode was 1.13 cm^2. In order to fire these oxide electrode layers, the cells were calcined for 8 h in air at 750 °C in a tube furnace. A slow heating and cooling rate of 1 °C min^{-1} was employed to allow controlled removal of the organic components and the pore former and to avoid warpage and cracking of the electrode layers. The final loadings of electrode oxide were calculated to be 7.3–8.3 mg cm^{-2} and their porosity was about 68 vol%.

Physico-chemical characterisation

The morphology of the electrolyte and the electrode layers was investigated by scanning electron microscopy (SEM) using a JEOL JSM-5600 instrument. Images of the exposed faces of the cells and of the cross-section of the electrode–electrolyte region were obtained. The crystallographic phase of the sintered

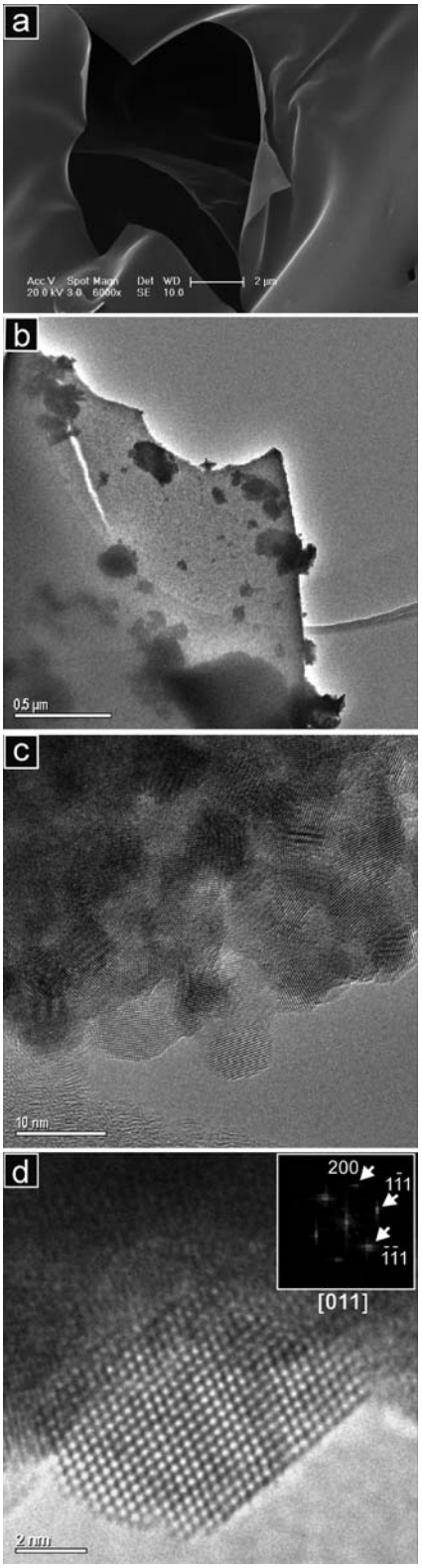

Fig. 1 SEM (a) and TEM images of Ce–Zr mixed oxides showing: (a–c) as-prepared thin, paperlike sheets of nanocrystals; (d) typical nanocrystal with digital diffraction pattern indexed to pseudo-Fluorite structure (inset).

electrodes was verified using XRD analysis on a Philips PW1050 diffractometer using Cu-Kα radiation and with a step size of 0.02° and a scan rate of 1 min^{-1} (both in 2θ). High grade silicon powder was used as a standard to allow for the instrument broadening correction.

Electrochemical characterisation

Electronic contacts were made to each of the two fired electrode layers using Ag mesh, Ag paste and Ag wire. The resulting symmetrical cells were tested in a quartz reactor operating at 1 atm pressure using a reactant gas of either 5% H_2 or 5% CH_4 (with balance Ar in both cases). Each reactant gas was humidified at 30 °C and supplied to the reactor at a flow rate of 100 ml min^{-1} (NTP). The temperature of the cell was monitored using a K-type thermocouple located 5 mm above the electrochemical cell. Electrochemical characterisation of the cells was carried out by Impedance Spectroscopy (IS) using a Solartron 1260 instrument operating in the two-electrode mode. All impedance spectra were collected in the frequency range of 10 MHz to 1 mHz at open circuit voltage (OCV) at a number of temperatures ranging from 400 °C to 700 °C. The applied signal was a sinusoidal potential of 10 mV amplitude. In the electrochemical tests the same procedure was followed for all electrode compositions. The temperature was ramped to 700 °C at 2 °C min^{-1} and the reactor was purged using N_2 at 100 ml min^{-1} for 0.5 h. The gas was switched to a flow of humidified 5% H_2 at 100 ml min^{-1} and this was passed through the reactor for 1 h. IS measurements were conducted in humidified 5% H_2 at descending temperatures from 700 to 400 °C, with a dwell of 20 min at each temperature before the IS spectra were recorded to allow the system to equilibrate. The reactor was held at 400 °C and purged using N_2 for 1 h. Humidified 5% CH_4 was then passed to the reactor at 100 ml min^{-1} for a period of 1 h. IS measurements were taken in the humidified 5% CH_4 at ascending temperatures from 400 to 700 °C. Again, dwells were built into the heating programme to allow equilibration of the system before recording the IS spectra. A blank symmetrical cell was also prepared using a GDC electrolyte pellet and Ag contacts but without the oxide electrode layers. This allowed the Ag contact and electrolyte impedances to be subtracted from the impedance plots of the test cells.

3. Results

3.1. Physico-chemical characterisation of symmetrical cells

As an example, the XRD pattern of the as-sintered Z50DC electrode layer after deposition on a GDC pellet is presented in Fig. 2. All the peaks match a tetragonal phase and are indexed accordingly in the figure. The absence of other peaks indicated that any additional phases were present below the detection limit of the XRD experiment (perhaps 1% for these high resolution patterns) and that the electrode material was therefore of high phase-purity. The Scherrer equation was used to estimate the mean particle size of the electrode material. The value obtained for Z50DC was 6.8 nm and was close to that of 7.2 nm obtained in the same way for the starting powder.[20]

Typical SEM images of the surface of a sintered GDC electrolyte pellet and of the cross-section of the Z50DC electrode–electrolyte interface in the symmetrical cell are shown in Fig. 3a and b, respectively. The GDC electrolyte appeared to be dense, as can be seen in Fig. 3b, and had a mean grain size of 1.1 μm. The electrode layer exhibited a highly porous microstructure in Fig. 3b and the interface between the electrode and electrolyte showed no separation, indicating good contact and adhesion between these two layers. The thickness of the electrodes was approximately 35 μm.

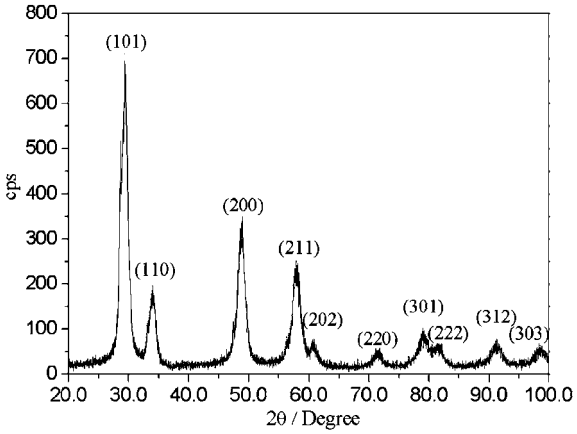

Fig. 2 XRD pattern of the Z50DC electrode after deposition on a GDC electrode pellet.

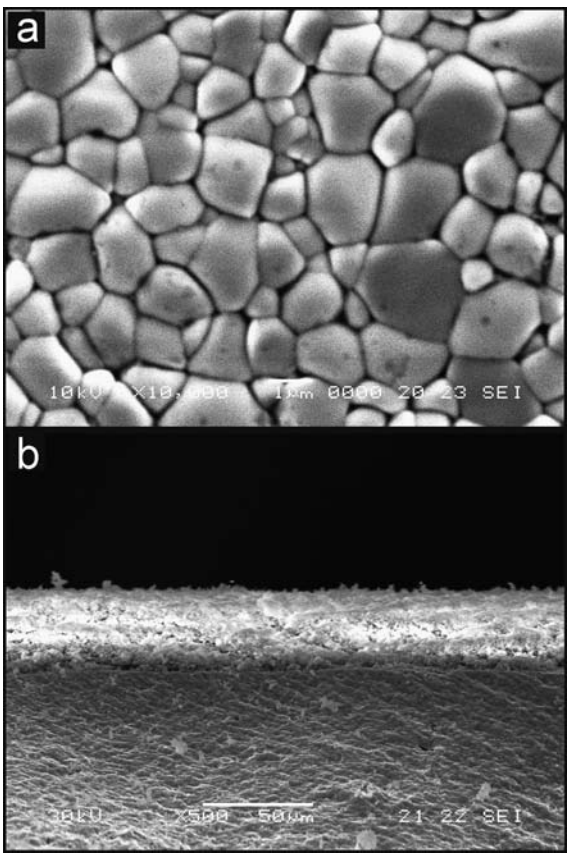

Fig. 3 Typical SEM images of (a) the GDC electrolyte surface and (b) the electrode–electrolyte region in cross-section.

3.2. Electrochemical characterisation

3.2.1. Ohmic Area-Specific Resistances of the ZDC electrodes. To obtain a standard impedance plot (an Nyquist plot), the frequency of the applied voltage is swept over a wide range and the real (Z_{re}) and imaginary components (Z_{im}) of the cell impedance are plotted against each other. Z_{re} and Z_{im} relate to the resistive and capacitive (or inductive) properties, respectively, of the cell under test. The left hand (high frequency) intercept of the impedance data with the Z_{re} axis gives the total ohmic resistance of the electrolyte, electrodes and all the external electronic resistances (the Ag contacts, wires). In the blank cell, which was prepared without oxide electrode layers, this intercept related to the ohmic resistance of only the electrolyte and the Ag contacts and external wires. By subtracting this intercept value from the intercept values obtained for the symmetrical test cells measured when each was operating under the same experimental conditions, the ohmic resistance of the electrode layers only could be obtained. Fig. 4 presents data extracted in this way in the form of Area-Specific Resistances (ASRs, to normalise for the geometric areas of the electrodes) in Arrhenius-type plots for all electrode compositions in the 5% H_2 atmosphere. It can be seen in these plots that the values are generally similar for all the ZDC compositions except for the Z90DC which shows a relatively high ASR, similar to that of the pure ceria composition.

3.2.2. Impedance spectroscopy of symmetrical cells with ZDC electrodes. Fig. 5a and b present impedance spectra for symmetrical cells with ZDC electrodes of all compositions, and of pure CeO_2, obtained at open circuit voltage (OCV) in humidified 5% H_2 at 600 °C and 700 °C, respectively. In order to conveniently compare the polarisation resistances, all the impedance spectra in Fig. 5 were left-shifted to the origin by subtracting the total ohmic cell resistance. For each cell, the remaining impedance feature consists of the overlapping of a minor high frequency contribution and a dominant low frequency feature. The distance between the intercepts at high (left) and low frequency (right) gives the electrode polarisation resistance and thereby an indication of the performance of the oxide electrodes. The electrode polarisation resistances of CeO_2 and Z90DC electrodes were similar at 700 °C (~0.33 Ω cm^2) and

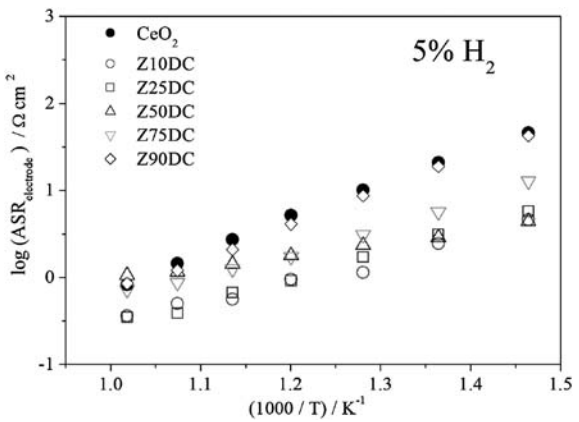

Fig. 4 The ohmic Area-Specific Resistances (ASRs) for all electrode materials in wet 5% H_2.

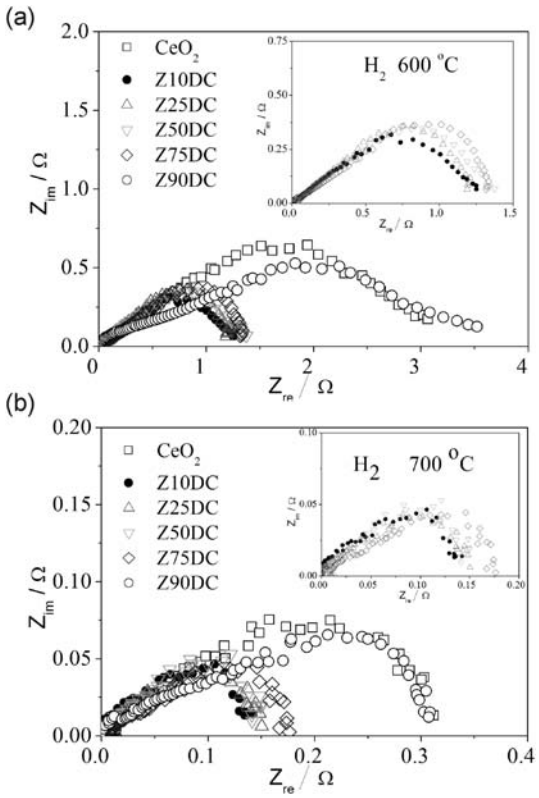

Fig. 5 Impedance spectra obtained for each electrode material in a symmetrical cell under wet 5% H_2 at (a) 600 °C and (b) 700 °C.

were 3.4 and 3.9 Ω cm^2, respectively, at 600 °C. These resistances were clearly higher than for all the other ZDC electrode materials tested. Electrodes with low Zr contents showed lower polarisation resistances of about 0.17 Ω cm^2 at 700 °C and 1.4 Ω cm^2 at 600 °C, approximately half of the corresponding values for CeO_2. It is clear from these results that the addition of ZrO_2 to the CeO_2 caused the anode performance in the H_2 atmosphere to be significantly enhanced.

Impedance spectra of symmetrical cells with ZDC electrodes tested in humidified 5% CH_4 at 600 °C and 700 °C, at OCV, are shown in Fig. 6. Again, the plots have been left-shifted in order to compare the polarisation impedances directly. The polarisation resistances were significantly higher than those measured in H_2. This can be attributed to the relatively low reactivity of CH_4 compared to that of H_2 at these intermediate temperatures.[6] For example, it was reported by Park and co-workers that CH_4 became more activated at higher temperature and that the performance gap between a cell using CH_4 and H_2 diminished when the cell was operated at higher temperature, *e.g.* at 900 °C.[4] As in 5% H_2, the Z90DC and CeO_2 electrodes presented the highest polarisation resistances. However, unlike in the H_2 atmosphere, in 5% CH_4 the Z90DC showed a much higher polarisation resistance, at 19 Ω cm^2, than that of CeO_2, which was 9.8 Ω cm^2. The polarisation resistances of ZDC with low Zr content were again the lowest and about half the value for CeO_2, at about 4.5 Ω cm^2. Those for Z50DC and Z75DC were slightly higher, at 5.4 and 5.8 Ω cm^2, respectively. This is in agreement with reports that the catalytic activity of pure ceria for total oxidation of methane can be enhanced by substituting ZrO_2 into

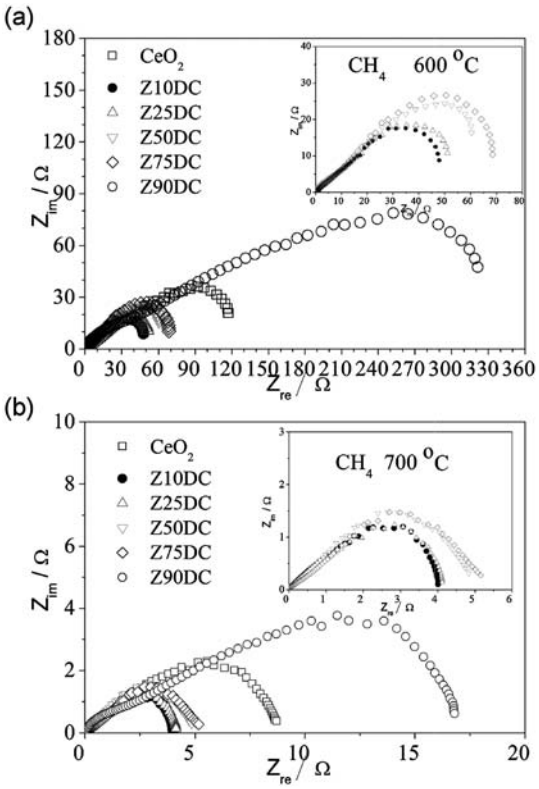

Fig. 6 Impedance spectra obtained for each electrode material in a symmetrical cell under wet 5% CH_4 at (a) 600 °C and (b) 700 °C.

ceria and that the best redox properties and highest OSC for ZDC was obtained at relatively low Zr content, with $x = 0.2$ to 0.4.[21,22] These results showed that by substituting Zr into CeO_2, the electrode performance can be increased significantly when using CH_4. Comparison of the polarisation resistance values in Fig. 5 and 6 also indicates a generally lower activity of the ZDC electrodes when operated in CH_4 compared to operation in H_2. This is expected, since CH_4 is generally accepted to be a more challenging SOFC fuel than H_2.

In summary, at both test temperatures and in both atmospheres the performance of the ZDC electrode materials, as indicated by the polarisation resistances, improved monotonically as Zr content decreased. The exception to this was the pure ceria, which showed the (joint) worst performance in 5% H_2 and the second worst in 5% CH_4.

4. Discussion

4.1 Electrode performance

The polarisation resistance values of the best ZDC electrodes—those with low Zr contents—imply very impressive performance. When converted into Area-Specific Resistances (ASRs), the best values were about 1.4 Ω cm^2 and 0.17 Ω cm^2 at 600 and 700 °C, respectively, in wet 5% H_2 and 4.5 Ω cm^2 in wet 5% CH_4 at 700 °C. Stormer *et al.*[23] investigated the impedance in a GDC/YSZ/GDC symmetrical cell. The electrode polarisation resistance was more than 20 Ω cm^2 in 9% H_2/91% N_2–3% H_2O, and more than 30 Ω cm^2 in pure CH_4, at 700 °C at OCV. Recently, Lv *et al.*[24] investigated $Ce_{1-x}Fe_xO_{2-\delta}$ (FDC, $x = 0.1$ and 0.2) as a new ceria-based anode material for SOFCs. The polarisation resistance measured at OCV in a symmetrical cell using LSGM as the electrolyte, and described as FDC/LSGM/FDC, was 0.975 and 0.577 Ω cm^2 in wet pure H_2 at 700 °C for $x = 0.1$ and $x = 0.2$, respectively. Barfod *et al.*[25] examined the impedance spectroscopy of an anode-supported Ni/YSZ symmetrical cell in 95% H_2/5% H_2O. The polarisation resistance was about 0.09 Ω cm^2 at 850 °C. They also reported the anode resistance of Ni/YSZ as 0.24 Ω cm^2 in 75% H_2/25% H_2O at 700 °C.[26] Murray *et al.*[2] developed a high performance direct-methane fuel cell with a ceria-based anode, which achieved a performance of 0.37 W cm^{-2} when operated on wet or dry pure CH_4 and air at 650 °C. The anode polarisation resistance was examined in a Ni–YSZ/YDC/YSZ/YDC/Ni–YSZ symmetrical cell. It was found to be about 1.2 and 1.0 Ω cm^2 at 600 °C for 97% CH_4/3% H_2O and 3% H_2/3% H_2O/94% Ar, respectively.

Tao and Irvine[27] developed the promising $La_{0.75}Sr_{0.25}Cr_{0.5}Mn_{0.5}O_3$ (LSCM) anode material and examined the anode performance in a half cell, which can be described as LSCM/YSZ/Pt. The best anode polarisation resistances were 0.51 Ω cm^2 and 0.87 Ω cm^2 at 900 °C in wet 5% H_2 and wet, pure CH_4, respectively, both with 3% H_2O. Even in wet, pure H_2, the anode polarisation resistance was 0.27 Ω cm^2 at 900 °C. Recently, Lay *et al.*[28] investigated the polarisation resistance of LSCM-based anodes in a symmetrical cell. The polarisation resistance of Ce-substituted LSCM was 0.2 and 1.6 Ω cm^2 at 900 °C at OCV in wet H_2 and wet CH_4, respectively. These authors also measured the polarisation resistance of LSCM without Ce substitution under the same conditions and obtained values of 2.3 and about 2.7 Ω cm^2 in wet H_2 and wet CH_4, respectively, at 900 °C at OCV. Chen *et al.*[29] studied the polarisation resistance of a 33% LSCM–67% GDC composite anode in a half cell, described as LSCM–GDC/YSZ/Pt, for application in an SOFC using methane. The anode polarisation resistance under a current density of 0.5 A cm^{-2} was 0.146 and 0.496 Ω cm^2 in wet, pure H_2 and wet, pure CH_4, respectively, at 850 °C. An *et al.*[30] examined the polarisation resistance of a Cu–ceria based anode in a whole cell using an LSGM electrolyte in three-electrode mode. At 700 °C, the anode polarisation resistance at a current density of 0.2 A cm^{-2} was 0.84 Ω cm^2 for dry pure H_2 and 1.4 Ω cm^2 for dry pure *n*-butane.

Some caution should be exercised when comparing polarisation resistance data obtained in symmetrical cells in different studies because of the possible effects of different microstructures and calcination histories of the electrode and electrolyte used and differences in experimental setup and operating conditions. Nevertheless, it is clear that ZDC does show very impressive performance when compared to the currently most promising candidate anode materials mentioned above for direct oxidation of hydrocarbon fuels in SOFCs, especially for application in IT-SOFCs.

4.2. Analysis and modeling of electrochemical impedance behaviour

The Gerischer-type impedance was derived in 1950s by Gerischer for a CE (chemical–electrochemical)-type electrode reaction. A review and detailed discussion can be found in a paper by

Boukamp and Bouwmeester.[15] Reports on the Gerischer-type impedance had been relatively rare until recently. The Gerischer-type response was observed in SOFC-related systems in several studies using symmetrical cells or half cells. Examples are a symmetrical cell with a porous mixed-conducting perovskite, $La_{1-x}Sr_xCoO_3$ (LSCO), as the cathode on a doped ceria electrolyte, described as LSCO/Ceria/LSCO, and tested in oxygen[18] and a 'half cell' consisting of a porous mixed-conducting Ca- or Sr-doped lanthanum chromium titanate perovskite (LACT, A = Ca, Sr) anode on a YSZ electrolyte with a Pt counter electrode, described as LACT/YSZ/Pt, and tested in wet, pure H_2.[31] Holtappels *et al.*[32,33] observed the Gerischer-type response in symmetrical cells using cermet electrodes of Ni–$Y_{0.2}Ti_{0.18}Zr_{0.62}O_{1.9}$ (Ni–YZT) on YSZ electrolytes when these were tested in humidified H_2. Adler[18] pointed out that for a mixed conducting electrode the traditional view of the charge transfer process as the rate-limiting step may not be the case in reality. He suggested that the oxygen reduction reaction on an LSCO electrode in a symmetrical cell was limited by a surface chemical exchange process and bulk oxygen diffusion. If the reaction region extending from the electrolyte/electrode interface was too small or too big, the impedance spectrum may deviate from the Gerischer-type response, giving rise to either a semicircle or a depressed semicircle. Gonzalez-Cuenca *et al.*[31] reported that Adler's view may not explain their results since the Gerischer impedance could only be observed in a thin mixed-conducting electrode (~20 μm) of chromite–titanate and not in the thicker one (100 μm) used in their experiments. Boukamp *et al.*[14] provided the expression for a double FFL-G impedance (eqn (1)) and its modelling procedure. Use of the FFL-G can result in a much better match between the model and the experimental data than for some other model components. He suggested that the surface diffusion of oxygen species to a triple phase boundary site limited the reaction process at the electrode under anodic conditions.

The use in the electrochemical cells described here of nanoparticulate, mixed-conducting electrode materials might be expected to give rise to fractal interfaces and to a highly distributed electrochemical process. Therefore, it seemed reasonable to attempt to fit our impedance data to both a Gerischer and to a FFL-G model. Fig. 7 shows a typical example of the experimental and fitted data, in this case for Z10DC electrodes at 700 °C in wet 5% CH_4 at OCV. The data were analysed by a subtraction method according to the procedure suggested by Boukamp *et al.*[14–16] The high frequency feature was fitted to an equivalent electrical circuit represented as $R_s(R_eQ)$. R_s represents the total ohmic cell resistance. The ohmic ASR values in Fig. 4 were derived from R_s. The resistance, R_e, and the constant phase element, Q, are in parallel and related to the electrochemical reaction process. This high frequency feature was subtracted from the data and the remaining dominant low frequency feature was fitted by non-linear fitting to the double FFL-G model (eqn (1)). As can be seen in Fig. 7, the FFL-G model clearly gave a much closer fit to the experimental data than a simple Gerischer element. This was the case for all impedance spectra obtained in this work.

It is interesting to plot the values of the main parameters used in this data-modelling procedure against temperature and against Zr content. The four parameters of most interest are the resistance of the electrochemical reaction process, R_e, the rate

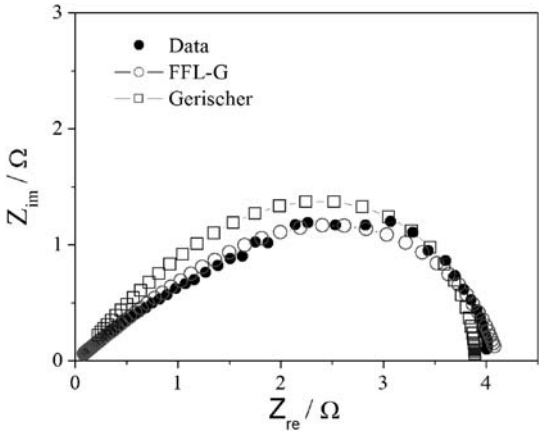

Fig. 7 Comparison between the experimental impedance spectrum (with high frequency feature subtracted) of the Z10DC electrode taken at 700 °C in wet 5% CH_4 with fits based on a simple Gerischer element and on the FFL-G (see text).

constant of the chemical exchange process, k, and two parameters related to the diffusion of the electroactive species, $Z_O/\tilde{D}_O^{1/2}$ and $L/\tilde{D}_O^{1/2}$. Z_O is the characteristic resistance, which is inversely related to oxygen ion concentration, c_o. $\tilde{D}_O$ is the corresponding coefficient of diffusion and L is the diffusion path length (see eqn (1) and (2)). As mentioned above, a Gerischer impedance is believed to be set up when a chemical exchange reaction (of rate constant, k) is coupled to a diffusion process (coefficient, $\tilde{D}_O$) and acts as a sink and source of species for the electrochemical reaction process (of resistance, R_e). In the materials studied in the present work, the diffusion terms relate to the chemical diffusion of oxygen ion species, by hopping between oxygen vacancies, in the electrode material. In addition to bulk oxygen ion diffusion, surface diffusion may also play a part, particularly in view of the large surface areas of these nanoparticulate ZDC and ceria materials. The chemical exchange must be a non-electrochemical process in which no charge transfer occurs but which involves species which are able to take part in the electrochemical reaction. Under the conditions of the work presented here, this will involve the (non-electrochemical) reaction, at the electrode surface, of oxygen-containing species—derived from O^{2-} ions—with species derived from CH_4 and H_2O. Charge transfer will occur in the electrochemical reaction process characterised by the parameter, R_e.

The four parameters identified above are presented in Arrhenius-type plots in Fig. 8 for the Z10DC electrode operating in wet 5% CH_4. The plots for all four parameters are close to linear, indicating Arrhenius-type behaviour is each case. With increasing temperature, the rate constant of the chemical process, k, increased and the resistance of the electrochemical reaction, R_e, decreased, as would be expected for thermally activated processes. This and the linearity of all of these Arrhenius plots were found to be general results for all electrode compositions and indicate that the fitting procedure carried out was valid and reliable.

For further insight, each of the four modelling parameters is plotted separately as a function of temperature in Fig. 9 for all of the ZDC electrodes and ceria. The activation energies of the model parameters were also estimated from these plots and are

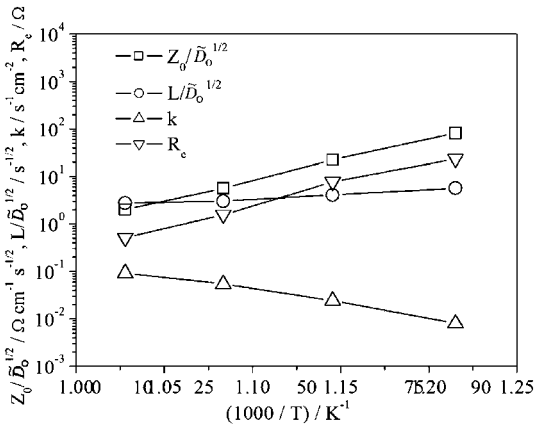

Fig. 8 Parameters of the FFL-G and the resistance associated with the electrochemical reaction, R_e, for the symmetrical cell with Z10DC electrodes in wet 5% CH_4 as function of temperature.

given in Table 1. Turning first to the parameter, $L/\tilde{D}_O^{1/2}$, Holtappels *et al.*[32,33] estimated the activation energy of $\tilde{D}_O$ in a Ni–YZT electrode system to be 70–80 kJ mol^{-1} by assuming that the diffusion length, L, was independent of temperature. Applying the same assumption, the activation energy of $\tilde{D}_O$ for the ZDC electrodes was found to be in the range, 60–110 kJ mol^{-1}, depending on composition. This range seems reasonable when compared with activation energy values obtained in some CeO_2—based electrodes such as for the oxygen isotope diffusion coefficient, D_O*, in CeO_2–YSZ (103 kJ mol^{-1})[34] and for oxygen ion conductivity in CeO_2–$GdO_{1.5}$–YSZ (50–95 kJ mol^{-1}).[35] Furthermore, if we assume L to be equal to the electrode thickness, as did Boukamp *et al.*,[14] we have $L = 35$ μm which gives values (from Fig. 8) of $\tilde{D}_O \sim 10^{-10}$ m^2 s^{-1}. This agrees with the value reported in the cited paper for a Ni–Ti-doped YSZ SOFC anode under reducing conditions at 800 °C. However, it is two to three orders of magnitude higher than the values obtained for D_O* in Secondary Ion Mass Spectroscopy (SIMS) measurements for the related oxide system, $[(CeO_2)_x(ZrO_2)_{1-x}]_{1-y}(YO_{1.5})_y$ (x = 0–1, $y = 0.2$ and 0.35).[34,36] This difference may be because these SIMS measurements were made under air, not under reducing conditions, or it may be an indication that surface diffusion played an important role in the results we present here. The latter point is reasonable, considering the nanoparticulate nature of the electrode materials. The activation energies of $Z_O/\tilde{D}_O^{1/2}$ are much higher than those for $L/\tilde{D}_O^{1/2}$. This could be explained by the expected exponential increase in $\tilde{D}_O^{1/2}$ with increasing temperature, while L in the term, $L/\tilde{D}_O^{1/2}$, also increased with temperature (*i.e.* unlike in the assumption made above), giving rise to a stronger overall temperature dependence for the term, $Z_O/\tilde{D}_O^{1/2}$, than for the term, $L/\tilde{D}_O^{1/2}$. Such temperature dependences have been reported by others.[32] Activation energy values for $Z_O/\tilde{D}_O^{1/2}$ are slightly lower for the intermediate compositions, and lowest for Z50DC. For the rate constant of the chemical exchange reaction, k, activation energy values showed a wider range of 52–110 kJ mol^{-1}, and the electrode compositions with the highest Zr content gave rise to the lowest values. A value of 125 kJ mol^{-1} has been reported for k in a Tb-doped YSZ anode.[15] In the case of the resistance of the electrochemical reaction, R_e, activation energy values showed little variation with changing electrode composition.

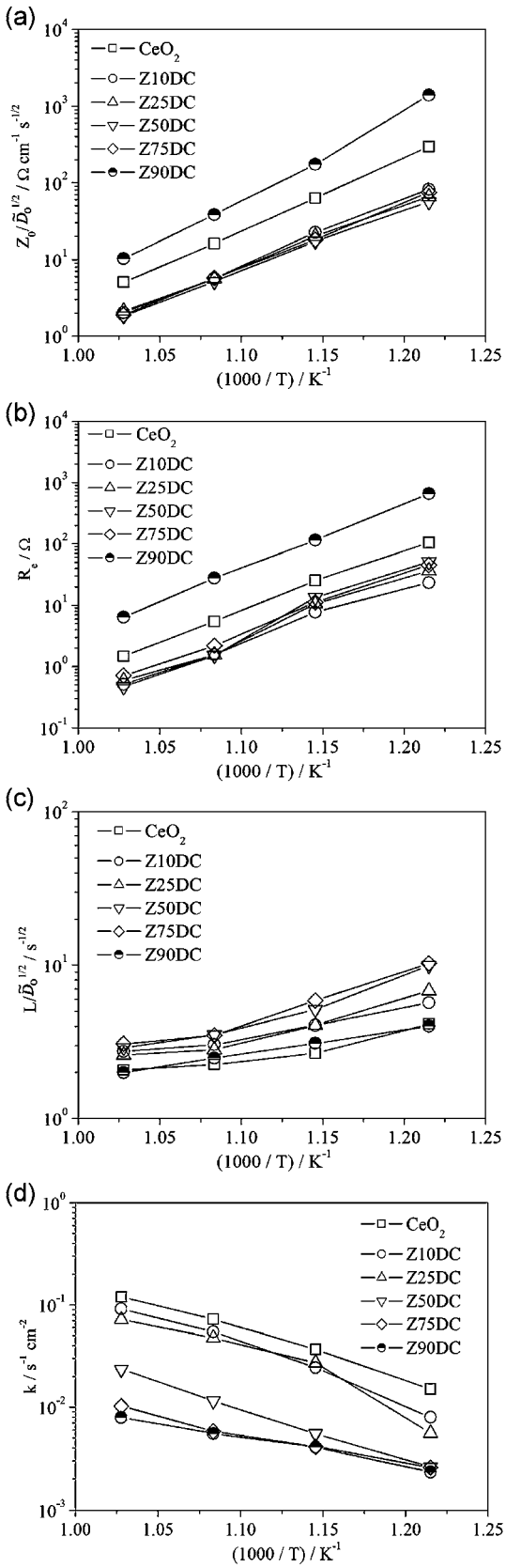

Fig. 9 Variation of the fitting parameters (see text) with inverse temperature for impedance spectra obtained in wet 5% CH_4: (a) $Z_O/\tilde{D}_O^{1/2}$, (b) R_e, (c) $L/\tilde{D}_O^{1/2}$ and (d) k.

Table 1 Activation energies (kJ mol^{-1}) for the Gerischer model parameters and for the electrochemical reaction resistance, R_e

Electrode composition	$Z_O/\tilde{D}_O^{1/2}$	$L/\tilde{D}_O^{1/2}$	k	R_e
CeO_2	−178	−30	92	−190
Z10DC	−166	−33	108	−173
Z25DC	−154	−43	110	−190
Z50DC	−152	−54	97	−216
Z75DC	−162	−55	59	−187
Z90DC	−216	−31	52	−203

Returning to Fig. 9, it is clear that electrode composition has an effect on each of the four parameters plotted and, furthermore, that these differences are maintained over the whole temperature range examined, 550–700 °C. To illustrate these effects, the four parameters are plotted against electrode composition for one temperature, 700 °C, under wet 5% CH_4 in Fig. 10. The parameter, $L/\tilde{D}_O^{1/2}$, shows very little change across the whole compositional range. The parameters, R_e and $Z_O/\tilde{D}_O^{1/2}$, are approximately constant at intermediate compositions but both show high values at both compositional extremes, for ceria and for Z90DC. Based on the discussions above, this indicates that the resistances of the electrochemical reaction process and of the diffusional process both have high values for these two compositions. Both of these effects would be detrimental to overall electrode performance (from eqn (2), high $Z_O/\tilde{D}_O^{1/2}$ would indicate a low diffusion coefficient, $\tilde{D}_O$). Finally, the rate constant of the chemical exchange reaction, k, increases monotonically with decreasing Zr content. This behaviour does not correlate directly with typically reported indices of the extent of reduction of $Ce_{1-x}Zr_xO_2$ materials in catalytic studies. The oxygen storage capacity (OSC), often expressed as moles O_2 stored by, or removed from, the material per gram of catalyst, and the concentration of Ce^{3+} ions (*e.g.* expressed as $[Ce^{3+}]/\{[Ce^{4+}] + [Ce^{3+}] + [Zr^{4+}]\}$) typically show high values at intermediate % Ce and low values for pure ceria and for low % Ce, as in the work of Daturi *et al.*[37] The parameter, k, is likely to be controlled by the availability of active surface sites for the chemical exchange reaction. The composition-dependence of k indicates that the surface concentration of Ce sites is the key factor. This is supported by the work of McIntosh *et al.*[38] who studied a number of lanthanide oxides for hydrocarbon oxidation with a view to their application in fuel cells. Light-off experiments for butane oxidation gave the activity trend: CeO_2 > Eu_2O_3 > Tb_4O_7 > Pr_6O_{11} > Sm_2O_3 >Yb_2O_3 > ZrO_2 ≈ La_2O_3. Fuel cell tests also showed CeO_2 to have the best performance and pure ZrO_2 nearly the worst. This indicated that Zr^{4+} had very poor activity for either catalytic or electro-catalytic butane oxidation, whereas Ce ions were very active (at least in pure CeO_2). These results are in broad agreement with the trend of k against % Ce in this work, where CH_4 was used, rather than butane.

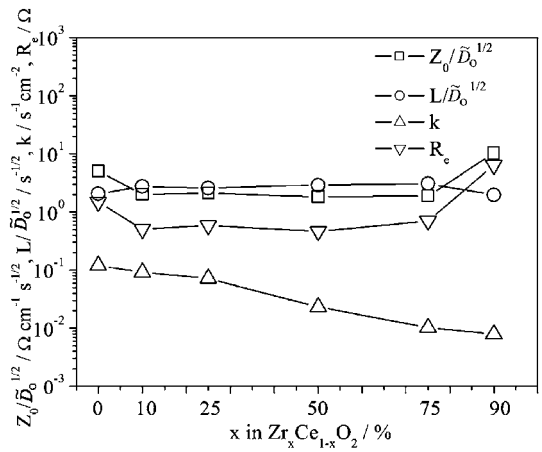

Fig. 10 Parameters of the FFL-G model and the electrochemical reaction resistance, R_e, at 700 °C in humidified 5% CH_4/95% Ar as a function of Zr content.

In Fig. 5 and 6 it can be seen that the Gerischer feature dominates the impedance spectra, masking the smaller feature associated with the electrochemical exchange reaction. This indicates that the overall performance of these electrodes can be attributed mainly to non-electrochemical factors, that is, to the combination of the parameter related to the diffusional process, $Z_O/\tilde{D}_O^{1/2}$, which was large for the end-members of the compositional series, and k, which increased with decreasing Zr content. This combination resulted in the electrode compositions with small, but non-zero, Zr contents (Z10DC and Z25DC) giving the lowest overall polarisation resistances and therefore the best performance. These are, therefore, the materials of most interest for application in fuel cell anodes.

5. Conclusions

In impedance studies on symmetrical electrochemical cells, a significant decrease in overall polarisation resistance was observed in $Ce_{1-x}Zr_xO_2$ anode materials compared with the pure ceria electrode under humidified 5% H_2 and humidified 5% CH_4. The only exception was for $Ce_{0.1}Zr_{0.9}O_2$ which showed performance inferior to CeO_2 under dilute methane and similar to CeO_2 under dilute hydrogen. The best performing electrode compositions were those with the lower Zr contents: $Ce_{0.9}Zr_{0.1}O_2$ and $Ce_{0.75}Zr_{0.25}O_2$. The anode performance of these electrodes compared very favourably with the currently most promising candidate anode materials applied in SOFCs for use with hydrocarbon fuels. The impedance spectra were analysed in terms of a double fractal finite length Gerischer impedance model. The model parameters indicated that overall electrode performance was dominated by non-electrochemical diffusion and chemical exchange reaction processes.

Acknowledgements

This work was funded by the UK Engineering and Physical Sciences Research Council and was performed within the EPSRC Supergen Fuel Cell Consortium (Phase One). We thank Prof. B. Boukamp for useful discussions on the Gerischer and FFL-G impedances.

References

1 B. C. H. Steele, *Nature*, 1999, **400**, 619.
2 E. P. Murray, T. Tsai and S. A. Barnett, *Nature*, 1999, **400**, 649.
3 S. Park, J. M. Vohs and R. J. Gorte, *Nature*, 2000, **404**, 265.
4 S. Park, R. Craciun, J. M. Vohs and R. J. Gorte, *J. Electrochem. Soc.*, 1999, **146**(10), 3603.

5 S. McIntosh, J. M. Vohs and R. J. Gorte, *J. Electrochem. Soc.*, 2003, **150**(10), A1305.
6 R. J. Gorte, S. Park, J. M. Vohs and C. Wang, *Adv. Mater.*, 2000, **12**, 1465.
7 H. Kim, S. Park, J. M. Vohs and R. J. Gorte, *J. Electrochem. Soc.*, 2001, **148**(7), A693.
8 H. He, J. M. Vohs and R. J. Gorte, *J. Electrochem. Soc.*, 2003, **150**(11), A1470.
9 R. Di Monte and J. Kaspar, *J. Mater. Chem.*, 2005, **15**, 633.
10 M. Boaro, A. Trovarelli, J.-H. Hwang and T. O. Mason, *Solid State Ionics*, 2002, **147**, 85.
11 S. Larrondo, M. A. Vidal, B. Irigoyen, A. F. Craievich, D. G. Lamas, I. O. Fabregas, G. E. Lascalea, N. E. W. de Reca and N. Amadeo, *Catal. Today*, 2005, **107–108**, 53.
12 K. Ahn, H. He, J. M. Vohs and R. J. Gorte, *Electrochem. Solid-State Lett.*, 2005, **8**(8), A414.
13 C. Lu, S. An, W. L. Worrell, J. M. Vohs and R. J. Gorte, *Solid State Ionics*, 2004, **175**, 47.
14 B. A. Boukamp, M. Verbraeken, D. H. A. Blank and P. Holtappels, *Solid State Ionics*, 2006, **177**, 2539.
15 B. A. Boukamp and H. J. M. Bouwmeester, *Solid State Ionics*, 2003, **157**, 29.
16 B. A. Boukamp, *Solid State Ionics*, 2004, **169**, 65.
17 J. Bisquert, *J. Phys. Chem. B*, 2004, **108**, 2322.
18 S. B. Adler, *Solid State Ionics*, 1998, **111**, 125.
19 R. O. Fuentes and R. T. Baker, *Int. J. Hydrogen Energy*, 2008, **33**(13), 3480.
20 R. O. Fuentes and R. T. Baker, *J. Phys. Chem. C*, 2009, **113**, 914.
21 F. Huber, H. Venvik, M. Ronning, J. Walmsley and A. Holmen, *Chem. Eng. J.*, 2008, **137**, 686.
22 D. Terribile, A. Trovarelli and C. de Leitenburg, *Catal. Today*, 1999, **47**, 133.
23 A. O. Stormer, P. Holtappels, H. Y. Tu and U. Stimming, *Materialwiss. Werkstofftech.*, 2002, **33**, 339.
24 H. Lv, H. Tu, B. Zhao, Y. Wu and K. Hu, *Solid State Ionics*, 2007, **177**, 3467.
25 R. Barfod, M. Mogensen, T. Klemensø, A. Hagen, Y. Liu and P. V. Hendriksen, *J. Electrochem. Soc.*, 2007, **154**(4), B371.
26 R. Barfod, A. Hagen, S. Ramousse, P. V. Hendriksen and M. Mogensen, *Fuel Cells*, 2006, **6**(2), 141.
27 S. Tao and J. T. S. Irvine, *Nat. Mater.*, 2003, **2**, 320.
28 E. Lay, G. Gauthier, S. Rosini, C. Savaniu and J. T. S. Irvine, *Solid State Ionics*, 2008, **179**, 1562.
29 X. J. Chen, Q. L. Liu, K. A. Khor and S. H. Chan, *J. Power Sources*, 2007, **165**, 34.
30 S. An, C. Lu, W. L. Worrell, R. J. Gorte and J. M. Vohs, *Solid State Ionics*, 2004, **175**, 135.
31 M. Gonzalez-Cuenca, W. Zipprich, B. A. Boukamp, G. Pudmich and F. Tietz, *Fuel Cells*, 2001, **1**(3–4), 256.
32 P. Holtappels, M. Verbraeken, U. Vogt, D. H. A. Blank and B. A. Boukamp, *Solid State Ionics*, 2006, **177**, 2029.
33 P. Holtappels, M. C. Verbraeken, D. H. Blank and B. A. Boukamp, *Proceedings of the 26th Riso International Symposium on Materials Science: Solid State Electrochemistry, Denmark*, 2005, p. 229.
34 H. Naito, N. Sakai, T. Otake, H. Yugami and H. Yokokawa, *Solid State Ionics*, 2000, **135**, 669.
35 N. M. Sammes and Z. Cai, *Solid State Ionics*, 1997, **100**, 39.
36 N. Sakai, K. Yamaji, Y. P. Xiong, H. Kishimoto, T. Horita and H. Yokokawa, *J. Electroceram.*, 2004, **13**, 677.
37 M. Daturi, E. Finocchio, C. Binet, J.-C. Lavalley, F. Fally, V. Perrichon, H. Vidal, N. Hickey and J. Kaspar, *J. Phys. Chem. B*, 2000, **104**, 9186.
38 S. McIntosh, J. M. Vohs and R. J. Gorte, *Electrochim. Acta*, 2002, **47**, 3815.